

Quantum Annealing of a Disordered Spin System

J. Brooke, D. Bitko, T. F. Rosenbaum

*The James Franck Institute and Department of Physics, The University of Chicago
Chicago, Illinois 60637*

G. Aeppli

AT&T Bell Laboratories, 4 Independence Way, Princeton, New Jersey 07974

Abstract

Traditional simulated annealing utilizes thermal fluctuations for convergence in optimization problems. Quantum tunneling provides a different mechanism for moving between states, with the potential for reduced time scales. We compare thermal and quantum annealing in a model disordered Ising magnet, $\text{LiHo}_{0.44}\text{Y}_{0.56}\text{F}_4$, where the effects of quantum mechanics can be tuned in the laboratory by varying a magnetic field applied transverse to the Ising axis. The results indicate that quantum annealing indeed hastens convergence to the optimum state.

In their presentation of simulated annealing, Kirkpatrick, Gelatt and Vecchi [1] described a fundamental connection between statistical mechanics and combinatorial optimization. Complex systems subject to conflicting constraints, from the traveling salesman problem and circuit design on one hand to spin glasses and protein folding on the other, are difficult to solve because of the vast number of nearly degenerate solutions. The introduction of a variable “temperature” permits the simulation to naturally subdivide a problem by energy scale, and as the temperature approaches zero the system settles into a local minimum (Fig. 1) that should be comparable to the ground state of the system.

If the settling is performed sufficiently slowly, then the minimum is guaranteed to be the ground state [2]. However, complex systems with many degrees of freedom may require impractically long annealing schedules to find the true lowest energy configuration. If barriers between adjacent energy minima are very high yet sufficiently narrow, it may be that quantum tunneling is a more effective means at energy minimization than pure thermal processes, with the potential to hasten convergence to the ground state.

As an example, consider the two-state spin system (“up” and “down”) used to introduce tunneling in quantum mechanics. The application of a magnetic field perpendicular to the up-down axis induces off-diagonal terms in the Hamiltonian, and enables tunneling between the two measured states. The assembly of a macroscopic number of such quantum spins on a lattice represents Feynman’s original concept [3] of a quantum mechanical computer. Information at the inputs (the original spin state of the system) undergoes a series of quantum mechanical operations, with the final set of ones and zeroes read at the outputs (the optimized, low energy spin state). Our experiment investigated a nontrivial optimization problem in statistical mechanics, namely that of finding the ground state for a ferromagnet

with a certain proportion of randomly inserted antiferromagnetic bonds (which favor antiparallel alignment of spins), and whether this problem can be solved more rapidly by quantum annealing than by classical thermal annealing. We started from the disordered, paramagnetic, high-temperature state in the dipolar-coupled Ising ferromagnet $\text{LiHo}_x\text{Y}_{1-x}\text{F}_4$, and read out the optimized low-temperature state using conventional magnetic susceptometry.

The Ising magnet $\text{LiHo}_x\text{Y}_{1-x}\text{F}_4$ in a transverse magnetic field H_t is the experimental realization of the simplest quantum spin model. The corresponding Hamiltonian (\mathcal{H}) is

$$\mathcal{H} = - \sum_{i,j}^N J_{i,j} \sigma_i^z \sigma_j^z - \Gamma \sum_i^N \sigma_i^x, \quad (0.1)$$

where the σ 's are Pauli spin matrices, the $J_{i,j}$'s are longitudinal couplings, and Γ is a transverse field. Given that the commutator $[\mathcal{H}, \sigma^z]$ is finite when $\Gamma \neq 0$, σ^z is no longer conserved and zero-point (quantum) fluctuations appear. These fluctuations increase with Γ , which tunes an order-disorder transition at $T = 0$. Our experiments are very different from traditional experiments on disordered magnets where fields are applied parallel to an easy direction for magnetization [4,5]. In particular, for Ising systems such as ferromagnetic $\text{LiHo}_x\text{Y}_{1-x}\text{F}_4$, a longitudinal field simply polarizes the spins at all T and removes the possibility of a ferromagnetic phase transition. By contrast, the transverse field Γ is not conjugate to the order parameter and retains a true phase transition. With this system we can directly compare the efficiency of quantum tunneling to classical thermal relaxation in finding the minima of a complicated energy landscape consisting of $N \sim 10^{23}$ spins.

In our experiments, the magnetic field H_t was applied perpendicular to the Ising axis (crystalline c axis) for the Ho spins. At low temperatures ($T < 1$ K), the only Ho^{3+} crystal field state which is appreciably populated is the ($H_t = 0$) ground-state doublet, which can be split in continuous fashion with great precision by the laboratory field H_t [6–9]. The splitting Γ plays the role of the transverse field in Eq. 0.1, whereas the doublet plays the role of the spin-1/2 eigenstates. For the present experiment, we selected a single crystal with 56% substitution of magnetically inert Y for Ho. The random dilution of magnetic by non-magnetic ions yields couplings between the magnetic ions of effectively random sign [10,11], which make the search for the ground state difficult in the rare earth lithium fluorides. The crystal was ground to a needle-like cylinder of aspect ratio three to minimize demagnetization effects. We suspended the cylinder from the mixing chamber of a helium dilution refrigerator inside the bore of an 80 kOe superconducting magnet, with the field direction oriented along the crystal a -axis (within 5°), perpendicular to the Ising axis (within 0.5°). A trim coil oriented along the Ising direction nulled any unwanted longitudinal field component. The protocol for comparing equilibration due to quantum tunneling and thermal hopping was straightforward. We annealed using both methods to the same point in the temperature-transverse field plane, and then measured the complete ac susceptibility, $\chi(f) = \chi'(f) + i\chi''(f)$, along the Ising axis with a standard gradiometer configuration and spectrum analyzer. Typical measuring frequencies (f) ranged between 10^0 and 10^5 Hz.

At low temperatures and large transverse fields, the mix of quantum mechanics and disorder converts $\text{LiHo}_{0.44}\text{Y}_{0.56}\text{F}_4$ from a classical ferromagnet with Curie temperature $T_c(H_t = 0) = 0.673$ K to a magnet with glassy, history-dependent behavior [12]. The $H_t - T$ phase diagram as well as two cooling protocols are shown in Fig. 1. The classical route (blue) crosses the phase boundary in zero transverse field, decreasing T from 0.800 K

to 0.030 K, and only then raising H_t to 7.2 kOe, whereas the quantum route (red), cools to 0.030 K in large transverse field (24 kOe), proceeding through the order-disorder transition with finite H_t and significant tunneling potential to the same nominal end point. The variation of T , H_t , and the real part of the magnetic susceptibility, $\chi'(f = 15 \text{ Hz})$, with time t are compared for the thermal and the quantum computation (Fig. 2). Remarkably, the magnetic susceptibility of the system at the identical place in the $H_t - T$ plane arrives at a different value depending on the annealing protocol. This difference survives to long times, at least on the order days.

Spectroscopy provides insight into the distribution and magnitude of relaxation times for spin reorientation. Fig. 3 shows $\chi'(f)$ over four decades of frequency at various points A to D in the phase diagram of Fig. 1. Spin relaxation proceeds conventionally, independent of annealing protocol, in the classical ferromagnet (Fig. 3A). As temperature is reduced to $T = 0.4 \text{ K}$ (Fig. 3B), differences start to emerge. The classically-cooled spectrum is approximately half a decade to the left of the quantum-cooled data; the quantum protocol has yielded a state with relaxation times a factor of three smaller than its classical counterpart. This effect increases dramatically on cooling deep into the ordered phase (Fig. 3C). As f decreases toward 1 Hz, $\chi'(f)$ grows logarithmically with roughly similar slopes for both annealing histories. The displacement between the two lines is now one and one-half decades; quantum cooling has produced a state for which the relaxation times are a factor of 30 faster than produced by classical cooling. Finally, keeping T fixed at 0.030 K and increasing H_t back into the paramagnet (Fig. 3D) narrows the spectroscopic response and restores the system's insensitivity to annealing method.

The logarithmic divergence of $\chi'(f)$ at $T = 0.030 \text{ K}$ is shown (Fig. 4) over nearly five decades in frequency. As H_t grows, the spectra move to the right; there is a spectacular acceleration of the relaxation. At the same time, the shift between the spectra obtained by quantum and classical cooling algorithms shrinks so that at 10.8 kOe quantum cooling renormalizes the relaxation times by only a factor of two.

The different time scales for classical and quantum annealing are also clearly evident in the imaginary part of the susceptibility, $\chi''(f)$ (Fig. 5), where the position of the peak response is the inverse of a typical relaxation time. Moreover, the low frequency dissipative response provides an additional basis for comparison. The quantum annealed data all converge and flatten at low frequencies, independent of transverse field destination at low T , while the classical curves appear to head towards separate low frequency, long time values. It is natural to associate the convergent state in the quantum computation with the ground state of the system. If the $\chi''(f, H_t)$ quantum response remains coincident and frequency independent as $f \rightarrow 0$, then by the Kramers-Kronig relation the real components, $\chi'(f, H_t)$, should be logarithmic in f , in agreement with what was measured directly (filled squares, Fig. 4). By the same token, the more diverse low frequency behavior of $\chi''(f)$ after classical cooling is reflected in the generally greater bowing and reduced parallelism between the classical $\chi'(f)$ curves of Fig. 4.

The logarithmically divergent $\chi'(f) \propto \ln(f/f_0)$, which characterizes the state G in the phase diagram of Fig. 1 implies that G is critical or marginally stable [13]. It is a nearly ferromagnetic state with equally probable fluctuations out of that state on all (long) time scales. Quantum and classical annealing protocols yield states which differ primarily in the characteristic frequency f_0 . The dramatically enhanced f_0 found for quantum cooling

shows that the addition of a tunneling term to the Hamiltonian (Eq. 0.1) yields a state with more rapid fluctuations. Most importantly, quantum cooling has allowed us to see more clearly and quickly that the ground state is likely a critical state: at $T = 0.030$ K and $H_t = 7.2$ kOe, there is only one decade of logarithmic behavior for classical cooling whereas there are already two and a half decades for quantum cooling.

Our experiments on $\text{LiHo}_{0.44}\text{Y}_{0.56}\text{F}_4$ directly demonstrate the power of a quantum mechanical term in the Hamiltonian for reaching a convergent solution, with obvious implications for designing simulated annealing computer algorithms [14]. They also raise more fundamental issues about strategies for the design of actual quantum computers. To date, the favored route has involved building a quantum computer qubit by qubit, taking advantage of the extraordinary sensitivity and isolation possible in modern nuclear magnetic resonance techniques [15,16]. Elaborate protocols for addressing and manipulating individual qubits are then required to perform computations. This work allows speculation about a less refined approach; cast the computation as a classical spin problem, which is then solved by a combination of thermal cooling and the blanket application of a transverse field. The transverse field, which controls the tunneling probability, is eventually driven to a low or zero value, and the solution can be read out in the form of the resulting and — at that point — frozen spin configuration

We have benefited greatly from discussions with P. Chandra, S. N. Coppersmith, and A. Ramirez. The work at the University of Chicago was supported primarily by the Materials Research Science and Engineering Center (MRSEC) Program of the NSF under award number DMR-9808595.

REFERENCES

- [1] S. Kirkpatrick, J. C.D. Gelatt, and M. P. Vecchi, *Science* **220**, 671 (1983).
- [2] S. Geman and D. Geman, *IEEE Trans. PAMI* **6**, 721 (1984).
- [3] R. P. Feynman, *International Journal of Theoretical Physics* **21**, 467 (1982).
- [4] J. A. Mydosh, *Spin Glasses: An Experimental Introduction* (Taylor & Francis, London, 1993).
- [5] D. H. Reich, T. F. Rosenbaum, G. Aeppli, and H. Guggenheim, *Phys. Rev. B* **34**, 4956 (1986).
- [6] W. Wu *et al.*, *Phys. Rev. Lett.* **67**, 2076 (1991).
- [7] W. Wu, D. Bitko, T. F. Rosenbaum, and G. Aeppli, *Phys. Rev. Lett.* **71**, 1919 (1993).
- [8] D. Bitko, T. F. Rosenbaum, and G. Aeppli, *Phys. Rev. Lett.* **77**, 940 (1996).
- [9] P. E. Hansen, T. Johansson, and R. Nevald, *Phys. Rev. B* **12**, 5315 (1975).
- [10] A. Aharony and M. J. Stephen, *J. Phys. C* **14**, 1665 (1981).
- [11] D. H. Reich *et al.*, *Phys. Rev. B* **42**, 4631 (1990).
- [12] D. Bitko, Ph.D. thesis, Univ. of Chicago, 1997.
- [13] P. Bak, C. Tang, and K. Wiesenfeld, *Phys. Rev. Lett.* **59**, 381 (1987).
- [14] T. Kadowaki and H. Nishimori, abstract available at <http://xxx.lanl.gov/abs/cond-mat/9804280>, 1998.
- [15] C. Monroe *et al.*, *Phys. Rev. Lett.* **75**, 4714 (1995).
- [16] N. A. Gershenfeld and I. L. Chuang, *Science* **275**, 350 (1997).

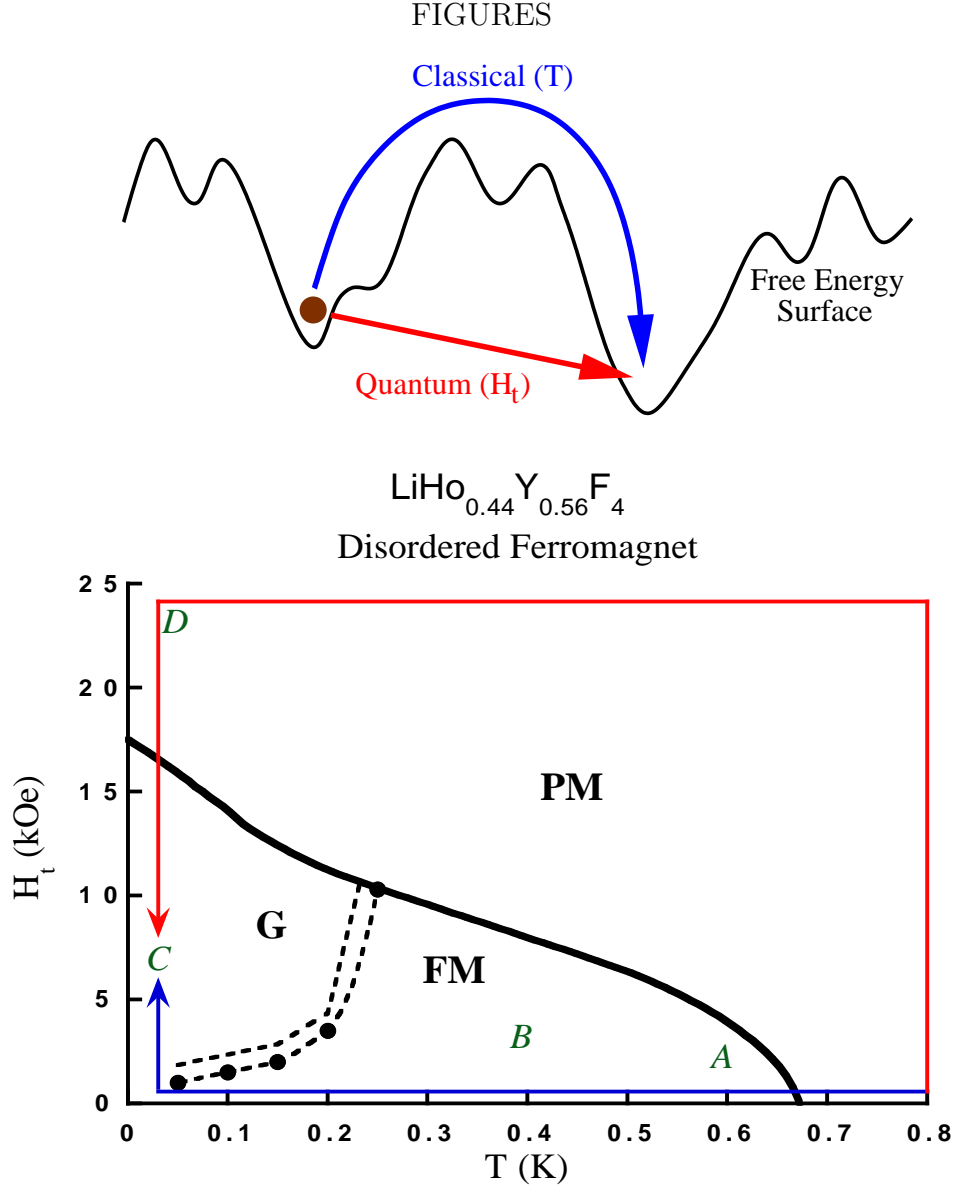


FIG. 1. Phase diagram showing quantum and classical annealing protocols. The quantum (red) and classical (blue) annealing protocols can provide different pathways through the free energy surface. PM = paramagnet, FM = ferromagnet, and G = glass, with the dashed line demarcating a dynamic crossover between manifestly FM and G regimes. A-D refer to specific points in the $H_t - T$ plane discussed in the text.

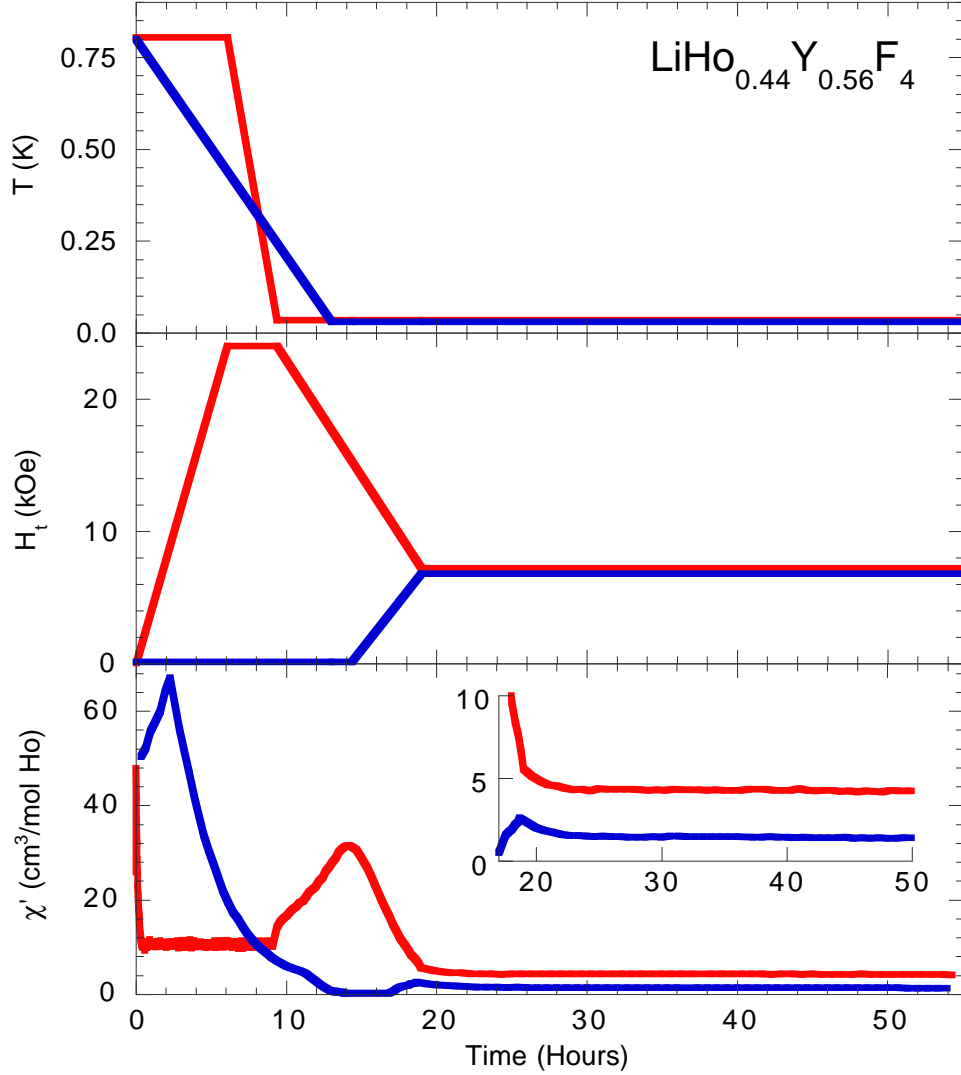


FIG. 2. Time evolution of the real part of the magnetic susceptibility, χ' , following classical (blue) and quantum (red) annealing histories at $f = 15$ Hz. Although the end point at $T = 0.03$ K and $H_t = 7.2$ kOe is identical, the long-time state of the system is different. The demagnetization limit for the sample geometry is $\chi' = 67$ cm³/mol Ho.

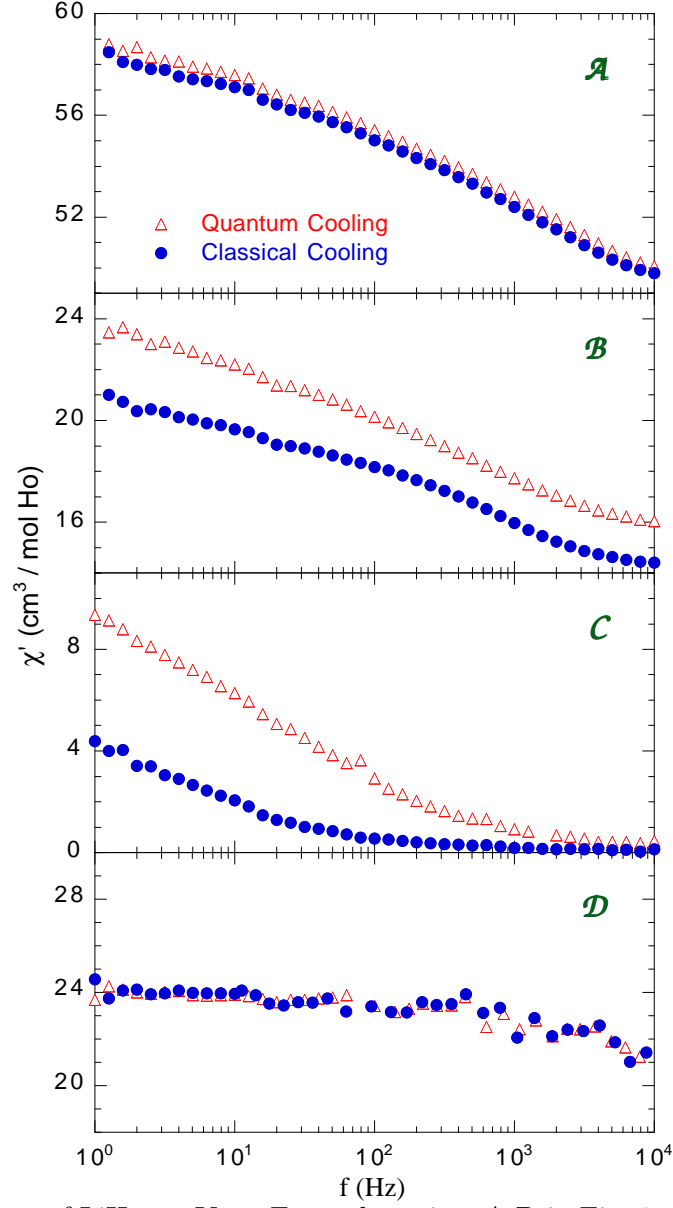


FIG. 3. Spectroscopy of $\text{LiHo}_{0.44}\text{Y}_{0.56}\text{F}_4$ at the points A-D in Fig. 1 after both quantum and classical computations. While the spectra begin together (A) in the classical ferromagnet, they start to diverge as T is lowered (B), until deep in the glassy phase (C) they exhibit widely different time scales and an unusual logarithmic dependence of χ' on frequency f . Crossing back into the quantum paramagnet (D) restores independence to the annealing history.

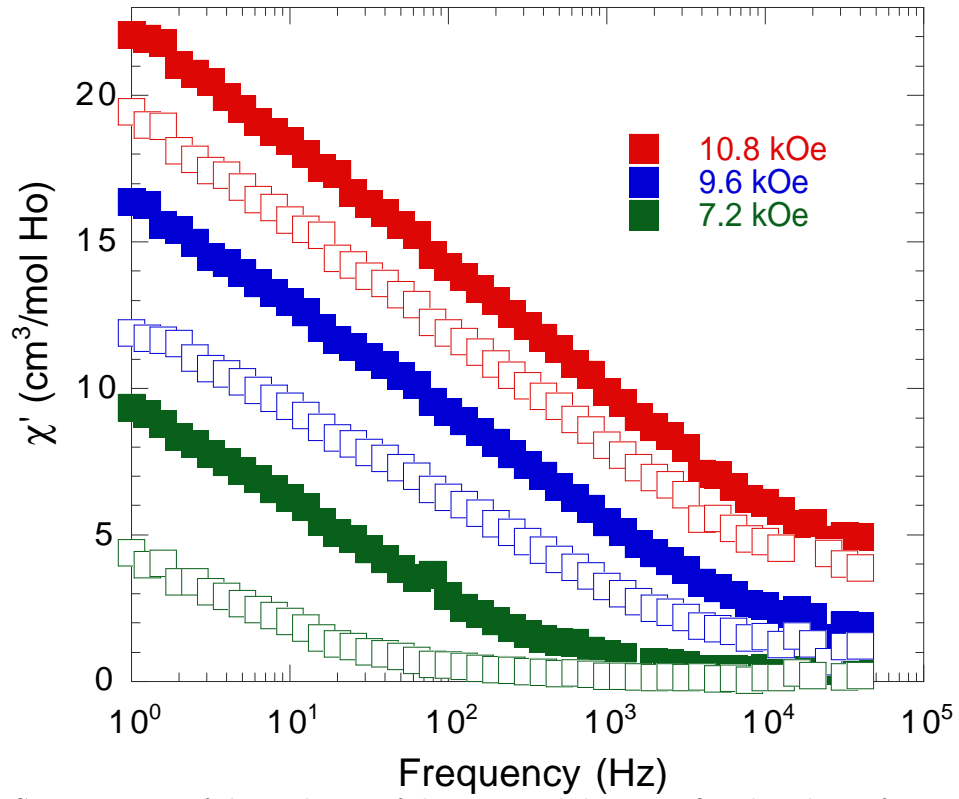


FIG. 4. Spectroscopy of the real part of the susceptibility over five decades in frequency, demonstrating a faster time scale for quantum annealing over its classical counterpart, as well as a well-defined logarithmic divergence at low frequencies.

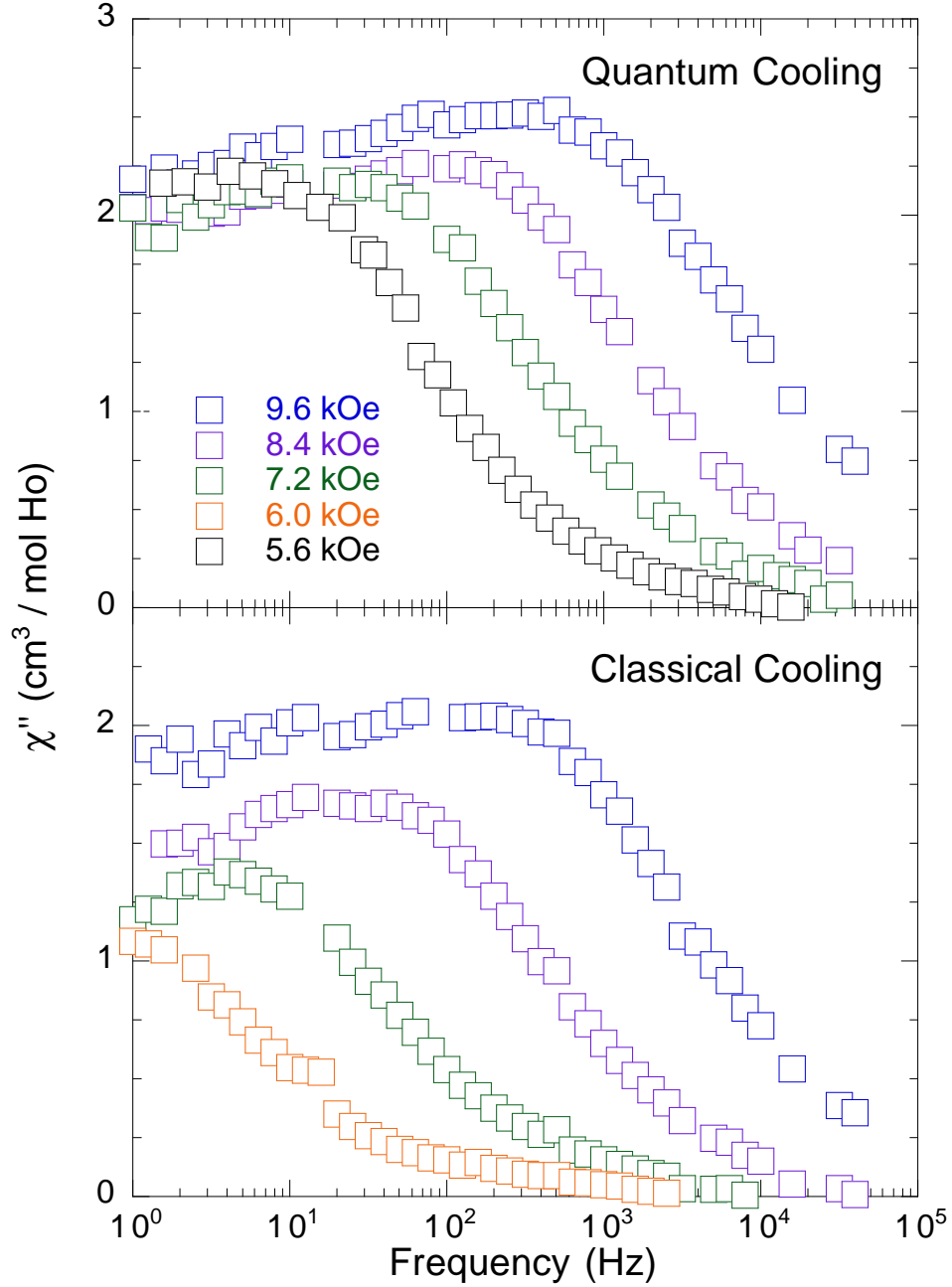


FIG. 5. The imaginary component of the susceptibility, $\chi''(f)$, not only serves to emphasize the faster typical times when quantum tunneling is featured, but reveals an apparent settling into the same state at low frequency independent of transverse field endpoint. The classical computation does not appear to possess such simple convergent properties.